Mechanisms of Electrocatalysis of Oxygen Reduction by Metal Porphyrins in Trifluoromethane Sulfonic Acid Solution

Qinggang He[1,], Tawanda Mugadza[2], GiSuk Hwang[1], and Tebello Nyokong[2,*]*

[1] Lawrence Berkeley National Laboratory, Environmental Energy Technologies Division, 1 Cyclotron Road, Berkeley, CA 94720, USA
[2] Department of Chemistry, Rhodes University, P.O. Box 94, Grahamstown, 6140, South Africa
[*]E-mail: QinggangHe@lbl.gov (Q. He), t.nyokong@ru.ac.za (T. Nyokong)

This study examines the oxygen reduction reaction (ORR) in a homogeneous catalyst system, comparing between the outer-sphere and inner-sphere electron-transfer mechanisms. The rate constants are measured using aqueous trifluoromethane sulfonic acid (TFMSA) and water-soluble M^* meso-tetra (pyridyl) porphine chloride complexes [M^*TMPyP, M^* = Fe(III), Co(III), Mn(III) and Cu(II)] at given pH and molar ratio of metal complexes to oxygen. An outer-sphere model consistent with Marcus theory explains that an outer-sphere electron transfer mechanism occurs in the activation-control region. However, higher rate constants than predicted suggests that a possible reaction pathway is a quasi-redox mechanism associated with the formation of an intermediate bond between $M^{'}$TMPyP [$M^{'}$ = Fe(II), Co(II), Mn(II) and Cu(I)] with O_2 followed by proton-activated decomposition. An increase in the catalyst turnover frequency was also observed upon addition of imidazole base, indicating the role of protonation is crucial to the ORR mechanism. The results are encouraging for replacement of platinum with non-noble metal-polymer complex systems for oxygen reduction in that the reorganization barrier for reaction pathway significantly decreases. The positive effect of proton activation on the catalytic activity of the homogeneous redox catalysts is of considerable interest for future studies. In a three-dimensional, molecular catalysis model, the predicted results using the measured reaction rate suggest that the non-noble metal catalysts can be used for practical electrochemical cell designs.

1. INTRODUCTION

Successful commercialization of proton-exchange-membrane fuel cells (PEMFCs) can be achieved by reduced cost, enhanced performance, and improved durability [1, 2]. In PEMFCs, the

largest overpotential results from the slow oxygen-reduction reaction (ORR) [3]. The large overpotentials also create parasitic heat, and this requires good thermal management system for the optimal operation that increases costs and worsens durability. The predominant use of platinum-based and platinum-group-metal (PGM) electrocatalysts is central to these issues [4, 5]. Thus, there are considerable incentives to examine alternative, less expensive, non-platinum catalysts with good ORR activity. Currently available non-PGM electrocatalysts can be broadly classified into pyrolyzed metal macrocycles with Metal-N_x reaction centers[6-9], first-row transition-metal based chalcogenides [10-14], and electron-conducting polymer-based structures [15-17]. These non-PGM catalysts exhibit slow ORR compared to the commercially available Pt-C electrodes. This sluggish kinetic rate is partially related to the structure of catalysts. The electrodes are highly porous for desired high specific-surface areas, but the resulting two-dimensional catalyst-layer structure limits the active reaction sites. With the porphyrin catalysts, for example, their poor solubility results in strong adsorption onto the carbon support with insufficient loading of catalyst and possible deactivation of the metal center [18-20].

Innovative electrode structures are required for both increased electrocatalyst surface area and full catalytic activity. Gasteiger and co-workers [21] have provided a review of the benchmark activities required for non-PGM catalysts for oxygen reduction. Their analysis concentrated on two significant factors, such as the turnover frequency (TOF) for the catalytic site in cycles per second, and the volumetric site density in active sites per volume. The recent surge of interest in enzyme catalysts has been prompted by their potential to meet these requirements. Some major progress on metal-complex systems reminiscent of enzymes has been reported to mimic the coordination environment [22] and proton-coupled electron-transfer process [23-25]. However, if the apparent benefits of enzyme catalysts [26-28] are to be realized in high-power fuel cells, then advances in catalyst design and synthesis are required to produce biomimetic catalysts designed for high turnover rates, and methods of incorporating molecular catalysts into membrane electrode assembly (MEAs) should be developed for the increase in the site density aiming at enhancing high current densities.

One method to increase site density is the attachment of the catalysts to the polymer layers [29]. The advantage of homogeneous redox catalysts is the ability to expand their site density relatively easily using a 3-D structure. The polymer redox layer includes molecular catalysts, and these result in a full access from all the species (electrons, protons, and substrates) for the increased reaction rate. The work was pioneered by Miller and Kerr [30, 31] and further developed by Saveant, Anson, and many other workers [32-34]. Here, we propose a polymer redox system having a non-noble metal catalyst impregnated with Nafion[®] as cathode catalyst layers of PEMFCs, as shown in Fig. 1. The bottom graph in Fig.1 shows that the non-noble metal catalyst (e.g. metal porphyrins) binds with sulfonic acid sites of Nafion[®] to form the 3-D molecular catalysis layers, and the polymer redox film is attached to the electrode surface. The electrons transport from the electrode through the catalytic sites, while the protons/oxygens migrate/diffuse along with the hydrophilic domains of the Nafion. The produced water molecules by the electrochemical reaction move to the redox polymer surface to form a parasitic liquid water layer. Note that the metal porphyrins can be chemically bonded with sulfonic acid sites of Nafion, and the catalyst unlikely moves around.[35] Thus, the electron transport is considered as hopping through bounded catalytic sites. The above redox polymer distributes to form a cathode catalyst layer as show in the up graph in Fig.1. The advantage of homogeneous redox catalysts

lies in the three-dimensional approach of substrates to the catalytic center as opposed to the two-dimensional approach to an electrode surface. Thus, although the rate determining activation energy may be the same, the pre-exponential factor is much higher due to the higher frequency of collisions that occur in the three dimensional approach of substrate to the catalyst.
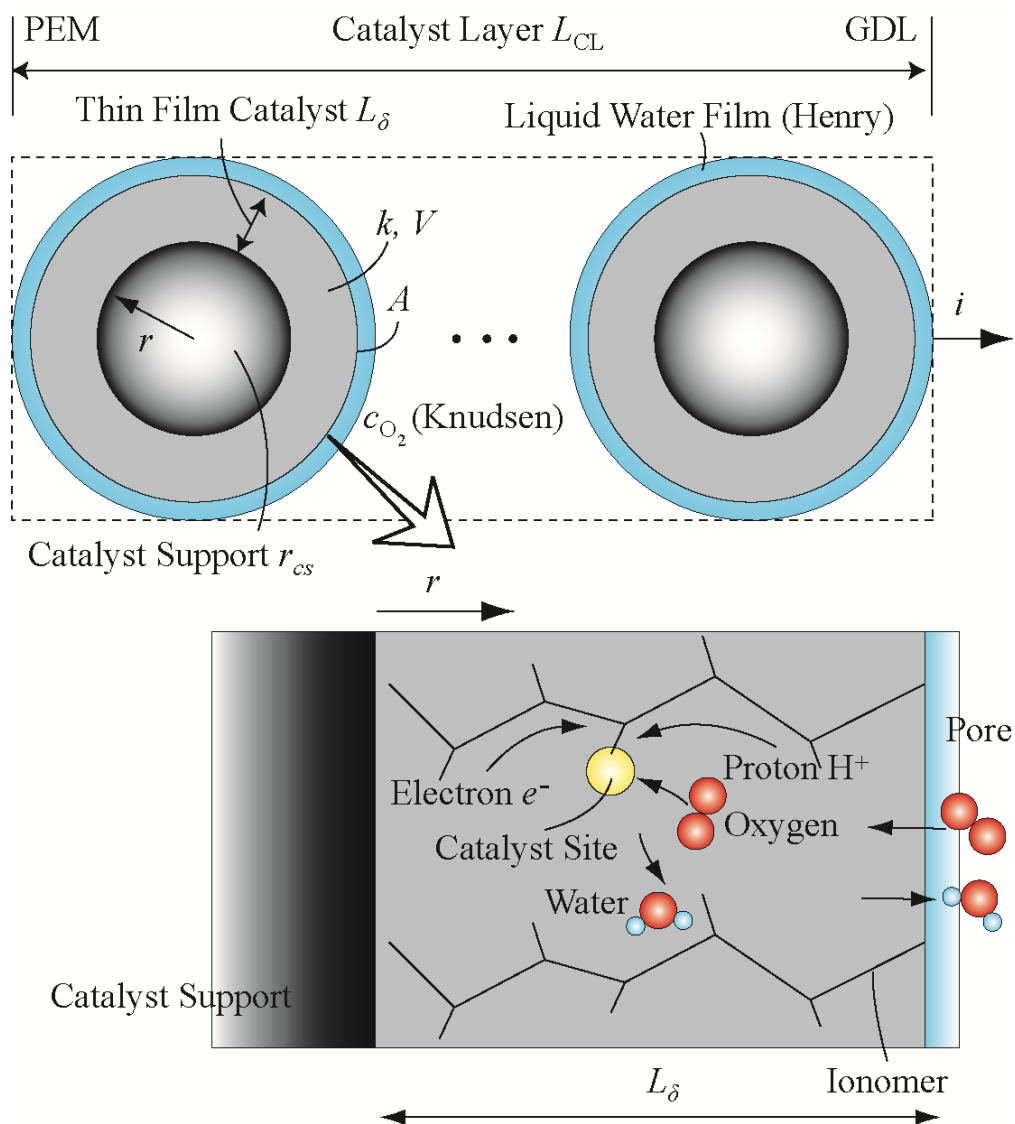

Figure 1. Schematic of a thin polymer-catalyst layer on the spherical catalyst support. The oxygen, proton, electron, and water transport in the thin polymer-catalyst layer are also shown.

To study the ORR kinetics of the homogeneous 3-D catalysis, water-soluble, metal-macrocycle compounds in trifluoromethane sulfonic acid (TFMSA) solution was used in this paper. TFMSA was chosen because its structure is similar to the typical PEMFC proton-exchange membrane, Nafion®. The kinetics of ORR by redox catalysis with water-soluble metalloporphyrins (Cu(II), Fe(III), Mn(III), Co(III) complexes) in TFMSA were studied using a rotating disk electrode and cyclic voltammetry at slow or moderate potential scan rates. The reaction pathways (outer- or inner-sphere catalysis) and reaction schemes were also explored.

2. EXPERIMENTAL

All metalloporphyrins were obtained from Frontier Scientific, Inc. and used as received. The metal meso-tetra(N-methyl-4-pyridyl)porphine chloride compounds have the same ligand structure with the central metal replaced by Fe, Mn, Co, and Cu respectively. They will be referred to as Fe(III)TMPyP, Mn(III)TMPyP, Co(III)TMPyP, and Cu(II)TMPyP hereafter. All other chemical materials were analytical grade and obtained from Sigma-Aldrich. The 0.1M trifluoromethanesulfonic acid (TFMSA) solution pH was determined to be 1 using a Beckman Coulter model 510 pH Meter.

Cyclic voltammetry (CV) and a rotating disk electrode (RDE) technique were employed to explore the kinetics of these metal porphyrin complexes in the absence and presence of O_2. Electrochemical measurements were conducted in a standard three-compartment electrochemical cell maintained at room temperature (20 to 25 ^{o}C) using a RDE setup from Pine Instrument Company connected to an Autolab bipotentiostat (PGSTAT302N). A glassy carbon electrode (diameter = 5.61 mm) from Pine Instrument Company was used as the working electrode, and a Pt wire was used as the counter electrode. A "no leak" Ag|AgCl reference electrode (Cypress Systems) was used. Before measurement, the RDE was successively polished with 1, 0.3, and 0.05-micron alumina slurry (Buehler, Lake Bluff, IL), and then cleaned with distilled water under sonication.

Differential pulse voltammetry (DPV) of the porphyrin complex in solution was done prior to in-situ spectroelectrochemical studies, using an Autolab potentiostat PGSTAT 302 (Eco Chemie, Utrecht, The Netherlands) driven by the general purpose Electrochemical System data processing software (GPES, software version 4.9). The step potential and the modulation amplitude were 4.5 mV and 25 mV respectively. A conventional three-electrode system consisting of a bare GCE (area = 0.071 cm^2), Ag|AgCl wire and a platinum wire were used as the working, pseudo reference and auxiliary electrodes, respectively. Shimadzu UV-2550 spectrophotometer was used to collect UV–vis spectral data. Spectroelectrochemical data were obtained by connecting a home-made optically transparent thin-layer electrochemical (OTTLE) cell to a Bioanalytical Systems (BAS) CV 27 voltammograph. All spectroelectrochemical experiments were performed in trifluoromethanesulphonic acid solution.

3. RESULTS AND DISCUSSION

A series of voltammograms with M*TMPyP (M*= Fe(III), Co(III), Mn(III) and Cu(II)) porphyrins dissolved in 0.1 M TFMSA were recorded at scan rates of 1 to 300 mV s^{-1}. The values of formal potential, E^0 can be calculated from the CVs (Fig.2) and the results have been tabulated in Table 1. Well defined redox couples corresponding to Fe(III)/Fe(II) [36, 37] and Mn(III)/Mn(II) [38] are obtained as shown in Figs. 2a and 2b.
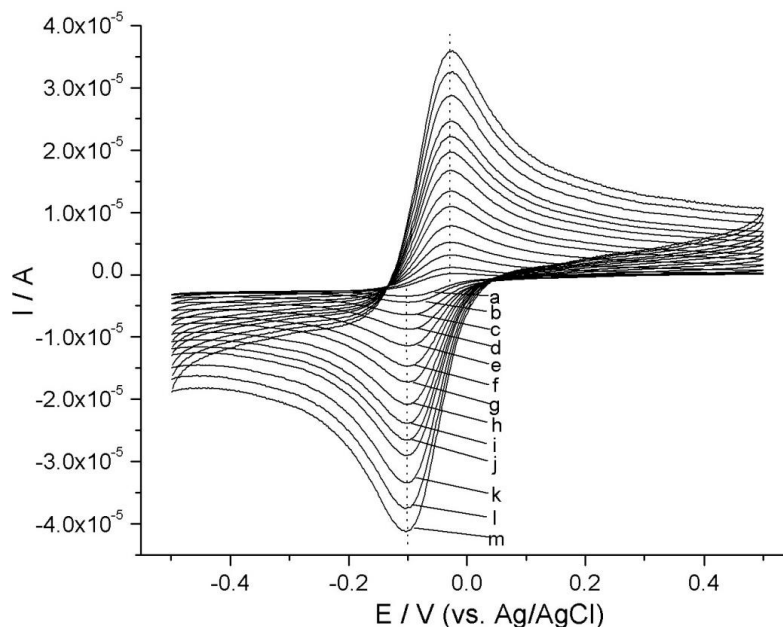
Figure 2a. Cyclic voltammograms on a glassy carbon in 0.1M TFMSA containing 0.8 mM Fe(III) complex recorded at different scan rates: (a) 1; (b) 2; (c) 5; (d) 10; (e) 20; (f) 50; (g) 75; (h) 100; (i) 125; (j) 150; (k) 200; (l) 250; (m) 300 mV s^{-1}
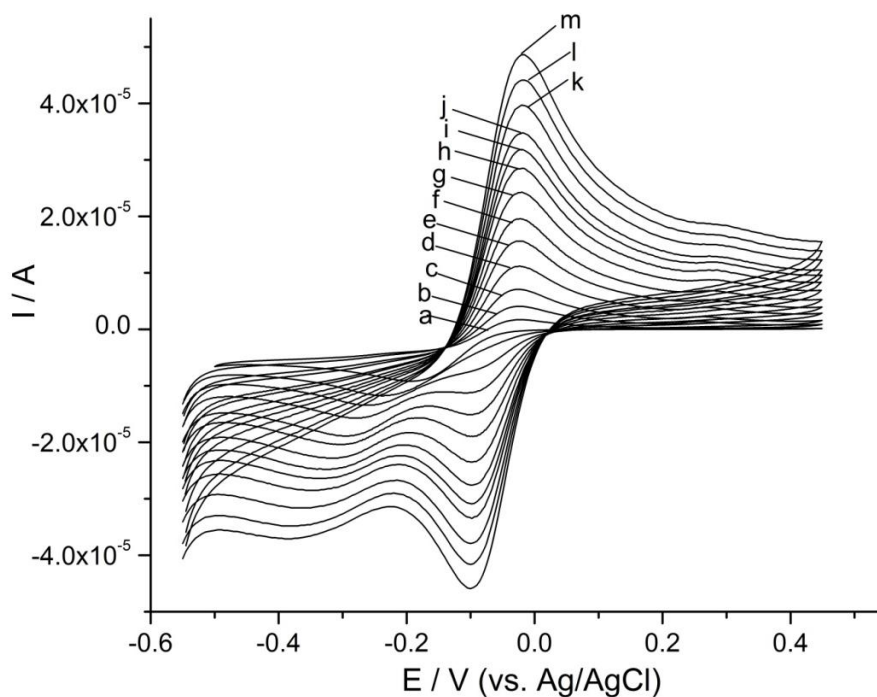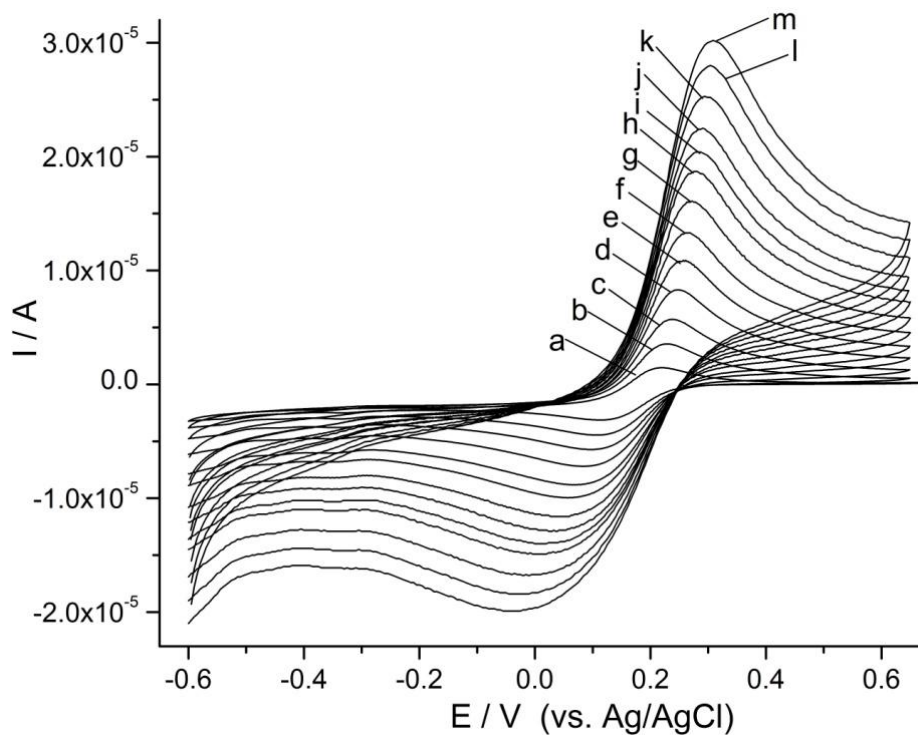

Figure 2b. Cyclic voltammograms on a glassy carbon in 0.1M TFMSA containing 0.8 mM Mn(III) complex recorded at different scan rates: (a) 2; (b) 5; (c) 10; (d) 20; (e)35; (f) 50; (g) 75; (h) 100; (i) 125; (j) 150; (k) 200; (l) 250; (m) 300 mV s^{-1}
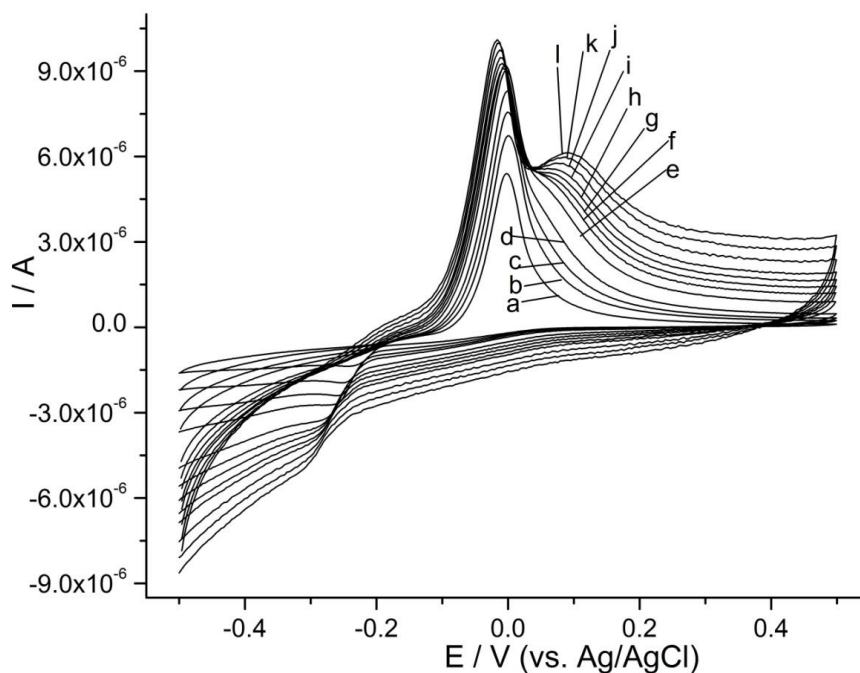
Figure 2c. Cyclic voltammograms on a glassy carbon in 0.1M TFMSA containing 0.8 mM Co(III) complex recorded at different scan rates: (a) 2; (b) 5; (c) 10; (d) 20; (e) 35; (f) 50; (g) 75; (h) 100; (i) 125; (j) 150; (k) 200; (l) 250; (m) 300 mV s^{-1}

Figure 2d. Cyclic voltammograms on a glassy carbon in 0.1M TFMSA containing 0.6 mM Cu(II) complex recorded at different scan rates: (a) 2; (b) 5; (c) 10; (d) 20; (e) 50; (f) 75; (g) 100; (h) 125; (i) 150; (j) 200; (k) 250; (l) 300 mV s^{-1}

Table.1 Kinetics parameter for 0.1M TFMSA + metal porphyrin complexes

Compound	E^0/V (vs.Ag/AgCl)	Number of electron transferred for ORR (n)	Reaction constant for reaction (c), k_1 ($M^{-1}s^{-1}$)
Co complex	0.1503	2.20	1.44E04
Fe complex	-0.065	4.0	6.04E04
Cu complex	-0.122	2.62	1.32E05
Mn complex	-0.049	2.49	4.81E04

These redox systems are reversible since the potential difference of anodic and cathodic peaks ($\Delta E_p = E_{pa} - E_{pc}$) is constant with various scan rates. In contrast, Fig. 2c shows that redox system of Co(III)TMPyP is quasi-reversible because of the gradual increase of ΔE_p as a function of the scan rate *v*. The reduction peaks of Cu(II)TMPyP (Fig. 2d) are more poorly defined than the other systems and there is a shoulder evolving along with the oxidation peak as the scan rate is relatively high (>50 mV s^{-1}). This indicates that the copper complex is related to adsorption on the glassy-carbon electrode strongly and irreversibly during the potential sweeps [39]. Interestingly, only the CV of Mn(III)TMPyP shows two reduction peaks. We highly suspect that these two peaks are correlated to formation of Mn(II) species with and without Cl$^-$ bonding.

Differential pulse voltammetry (DPV) and in-situ spectroelectrochemistry studies were done in the absence and presence of 120 mM KCl in order to elucidate the origin of the second reduction peak seen in Fig.2b. In DPV studies, from Fig. 3, two peaks were observed in both cases, ones at around -0.25 V (I) and broad ones in the range -0.35 to -0.43 V (II) versus Ag|AgCl. The peak at -0.25 V is due to the Mn(III)/Mn(II) reduction process [40, 41]. This peak exhibits larger peak currents with no significant shifts in peak potentials on introduction of 120 mM KCl.
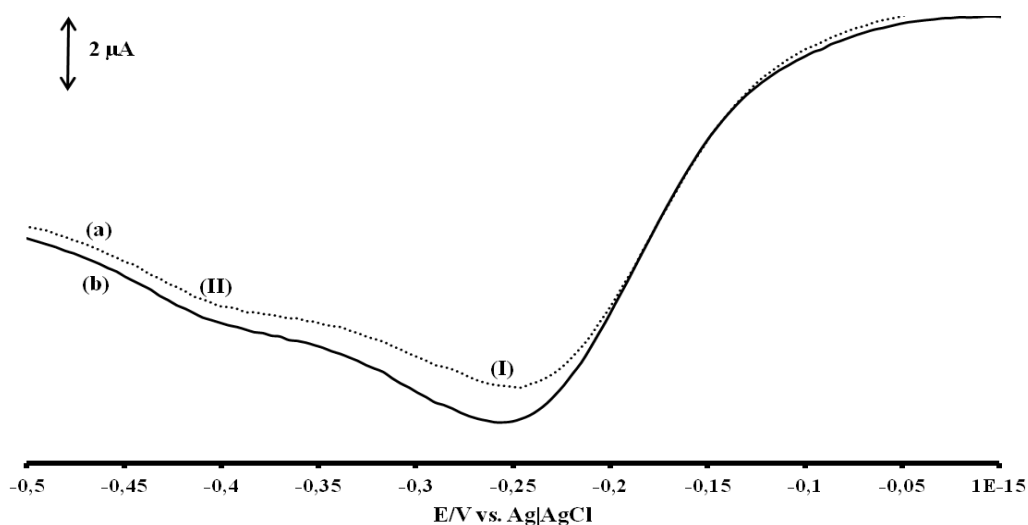

Figure 3. Reduction Differential Pulse voltammograms, for Mn(III)TMPyP in 0.1 M TFMSA in the absence (a) and presence (b) of 120 mM KCl. Both solutions were purged with nitrogen gas. Step potential = 4.5 mV, Modulation amplitude = 25 mV

The presence of the broad peak (II) is an indication of the existence of different manganese porphyrin species, most probably the Mn(II)-Mn(III)-Mn(II) porphyrin trimers that are further reduced to give Mn(II)-Mn(II)-Mn(II) complexes [40]. Manganese porphyrins therefore appear to follow an "Electrode-Chemical-Electrode" (ECE) mechanism, while the other M*(III)TMPyP complexes follow the "Electrode-Chemical" (EC) steps [42, 43]. However, irrespective of the reduction mechanism that is followed, the presence of these Mn(II) species in solution encourages the catalytic reduction of oxygen, therefore the oxygen reduction mechanism on Mn(II)TMPyP is not affected.

Spectroelectrochemistry was used to confirm the peak assignments made from DPV studies on Mn(III)TMPyP (Fig. 3). The behavior of Mn(III)TMPyP was observed to be different in the TFMSA in the absence and presence of KCl. Figs 4a and 4b show the observed spectral changes in the absence and presence of KCl, respectively. In both cases the absorption band at 461 nm was reduced (Figs. 4a and 4b). This is attributed to ionic interactions (TFMSA anions for the former, Fig. 4a and TFMSA anions and Cl$^-$ ions for the latter, Fig. 4b) which change the geometry of the complex, causing the observed decrease in optical absorption [40]. Due to the presence of Cl$^-$ (120 mM) ions, blue shifting was observed from 557 nm (Fig. 4a) to 547 nm (Fig. 4b) for Mn(III)TMPyP , a confirmation of the interaction between the porphyrin metal centre and the chloride ions. In the absence of Cl$^-$ ions free Mn(II) ions in solution forms Mn(II)-O$_2$-Mn(II) oxo-bridged porphyrins with residual oxygen despite of the purging, which could be responsible for the absorption band at 510 nm, Fig. 4a. This band cannot be attributed to Mn(II)-Mn(III)-Mn(II) species as shown by the presence of two reduction bands (Fig. 3). The absence of this band (Fig. 4b) in the presence of 120 mM KCl confirms the presence of the non-ionized (Cl)Mn(II)TMPyP species in solution, therefore the formation of Mn(II)-O$_2$-Mn(II) oxo-bridged porphyrin species is not feasible.
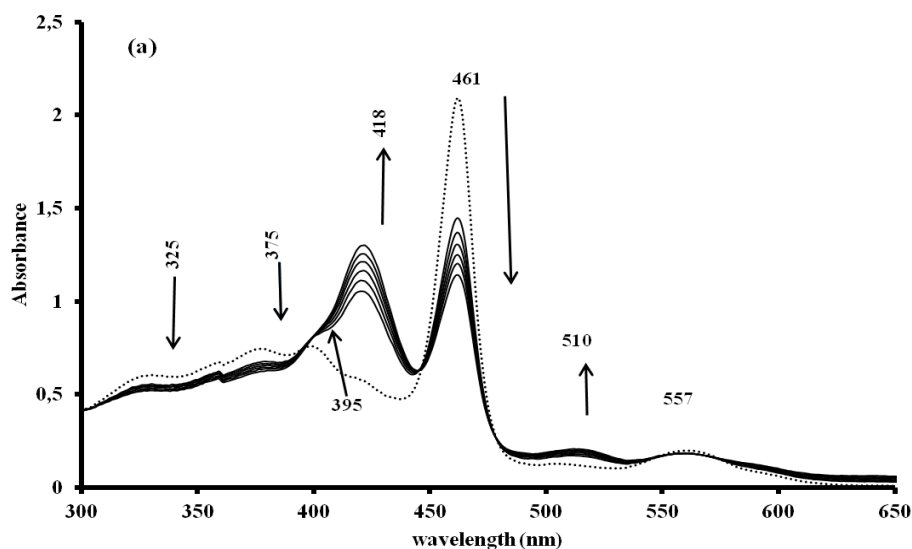

Figure 4a. UV−vis spectral changes observed in an OTTLE cell for the Mn(III)TMPyP (in 0.1 M TFMSA) reduction peak II (Fig. 2b) at E = -0.5 V in the absence of 120 mM KCl. All the spectral studies were done in degassed solutions. Dashed line (spectrum before electrolysis) and bold line (spectrum after electrolysis).
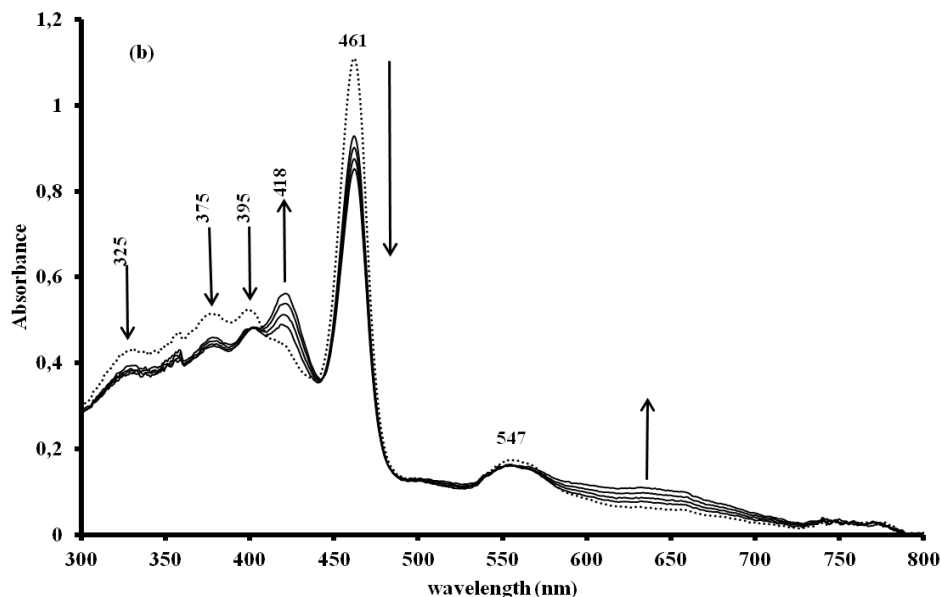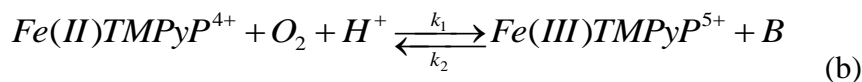
Figure 4b. UV–vis spectral changes observed in an OTTLE cell for the Mn(III)TMPyP (in 0.1 M TFMSA) reduction peak II (Fig. 2b) at E = -0.5 V in the presence of 120 mM KCl. All the spectral studies were done in degassed solutions. Dashed line (spectrum before electrolysis) and bold line (spectrum after electrolysis).

The vibronic band at 395 nm disappeared completely in the absence of 120 mM KCl, Fig. 4a. In the presence of Cl⁻ ions the same band at 395 nm decreased gradually. The bands at 418 nm and 461 nm increased and decreased respectively. The appearance of diffuse isosbestic points in both cases suggests the presence of more than one species in solution. From the differential pulse voltammetric and spectroelectrochemical studies, upon reduction Mn(III)TMPyP complexes speciate into a variety of new compounds. Relative to other M*TMPyP complexes in this study, the presence of the Cl⁻ ions does offer a different reduction pathway for oxygen on Mn(III)TMPyP electrodes.

The electrochemical response of the metal-porphyrin systems was perturbed after purging O_2 through the TFMSA electrolyte. Figs. 2 and 5 show that the onset potential for the ORR is identical to the potential at which the M*TMPyP are reduced. This indicates that the ORR process follows a general catalytic-regeneration mechanism [42-44]. Using Fe(III)TMPyP as an example, the reactions steps are postulated in reactions (a) to (c):

$$\text{Fe(III)TMPyP}^{5+} + e^- \leftrightarrow \text{Fe(II)TMPyP}^{4+} \qquad \text{(a)}$$

$$Fe(II)TMPyP^{4+} + O_2 + H^+ \underset{k_2}{\overset{k_1}{\rightleftharpoons}} Fe(III)TMPyP^{5+} + B \qquad \text{(b)}$$

$$\text{B} \rightarrow \text{product} \qquad \text{(c)}$$
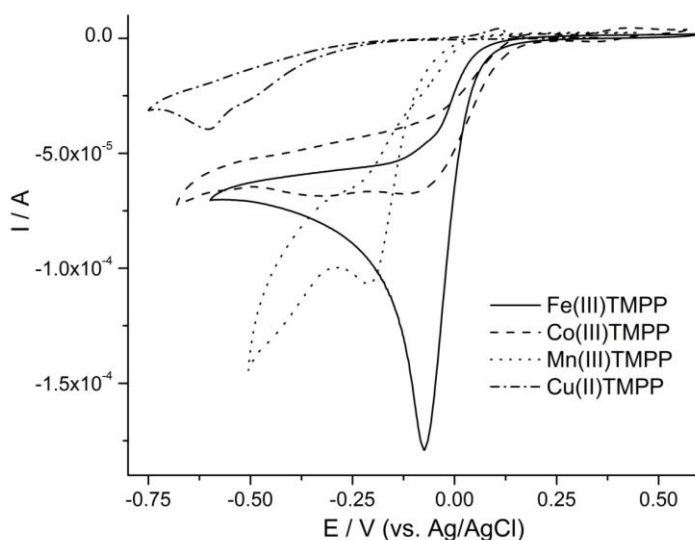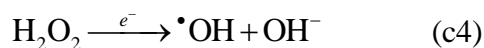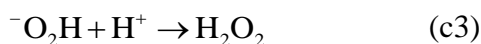
where B is a reaction intermediate.

Figure 5. ORR Cyclic voltammograms on a glassy carbon in 0.1M TFMSA containing 0.8 mM Fe(III)TMPyP, 0.8 mM Co(III)TMPyP, 0.8 mM Mn(III)TMPyP and 0.6 mM Cu(II)TMPyP in the presence of O_2, scan rate = 50mV s^{-1}

When reaction (c) is much faster than the reverse reaction (b), all of B will disappear by reaction (c) and the catalytic current will be determined solely by the rate of reaction (b). Assuming B as the initial species of the oxygen reduced by Fe(II)TMPyP is superoxide ion [45], $O_2^{\bullet-}$, the reaction (c) may include a series of reactions as follows:

$$O_2^{\bullet-} + H^+ \rightarrow {}^{\bullet}O_2H \qquad\qquad (c1)$$

$$ {}^{\bullet}O_2H \xrightarrow{\;e^-\;} {}^-O_2H \qquad\qquad (c2)$$

$$ {}^-O_2H + H^+ \rightarrow H_2O_2 \qquad\qquad (c3)$$

$$H_2O_2 \xrightarrow{\;e^-\;} {}^{\bullet}OH + OH^- \qquad\qquad (c4)$$

$$ {}^{\bullet}OH \xrightarrow{\;e^-\;} {}^-OH \qquad\qquad (c5)$$

$$ {}^-OH + H^+ \rightarrow H_2O \qquad\qquad (c6)$$

In this theme, $O_2^{\bullet-}$ is produced as an intermediate and reacts with a proton. To examine the validity of this outer-sphere electron transfer mechanism, one can derive the rate constant k_1 for oxidation of Fe(II)TMPyP^{4+} in reaction (b) from the ratio of peak currents I_{CAT} / I_D as a function of the concentration of C_p (p = Fe(III)TMPyP). In this case, I_D is the peak current for a solution of

Fe(III)TMPyP alone, I_{CAT} is for the reduction of Fe(III)TMPyP in the presence of O_2, and v is the potential scan rate. The dimensionless plots for estimating the value of k_1 for reactions with a general "Electrode-Chemical" (EC) mechanism have been well established in Saveant *et al*'s series of publications [42-44, 46, 47]. The case involving *n* electrons can be handled by calculating $I_{CAT} / n\gamma I_D$ ($\gamma = \dfrac{C_{O_2}}{C_p}$) and using the working curve for *n*γ.

To obtain the number of electrons (*n* value) transferred in the reaction of O_2 reduction, RDE experiments were conducted in O_2 saturated 0.1 M TFMSA solution. The ORR curves in 0.1 M TFMSA + 0.8 mM Fe(III)TMPyP and the other metal porphyrins at different rotation rates are presented in Fig. 6. CVs recorded in Argon-purged solution were subtracted from the ORR polarization current density at the same sweep rate to eliminate the influence of the irreversible adsorption of metal complexes and charge of the electrical double layer. From the RDE data in Fig. 6, the Koutecky-Levich plots of $1/j$ vs. $1/\omega^{1/2}$ were calculated according to Equations (1) and (2) and the results are displayed in Fig. 7. The values of the B coefficients for O_2 reduction in 0.1 M TFMSA + Fe(III)TMPyP and other metal porphyrins were determined from the slope of the plots in Fig. 7. The results match very well with those reported in the literature [48, 49] and can be found in Table.1.

$$\frac{1}{j} = \frac{1}{j_k} + \frac{1}{j_d} \tag{1}$$

$$j_d = B\omega^{1/2} = 0.620nFD^{2/3}C_0 v^{-1/6}\omega^{1/2} \tag{2}$$

Where j_k is the kinetic current density; j_d is diffusion limiting current density; *n* is the number of exchanged electron; ω is the angular frequency of rotation, $\omega = 2\pi f/60$; *f* is RDE rotation rate in rpm; F is the Faraday constant (96485 C mol^{-1}); *D* is the diffusion coefficient of the molecular O_2; v is the kinematic viscosity and C_O is the concentration of oxygen molecules.
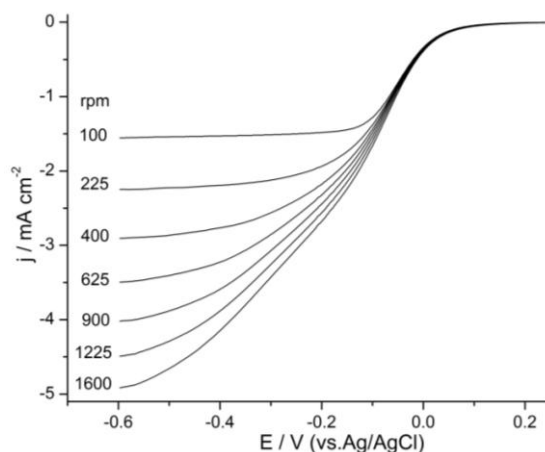

Figure 6a. Disk currents density (based on the geometric area of the glassy carbon electrode) at different rotation rates during the ORR in 0.1M TFMSA + 0.8 mM Fe(III)TMPyP. Scan rate: 20mV s^{-1}
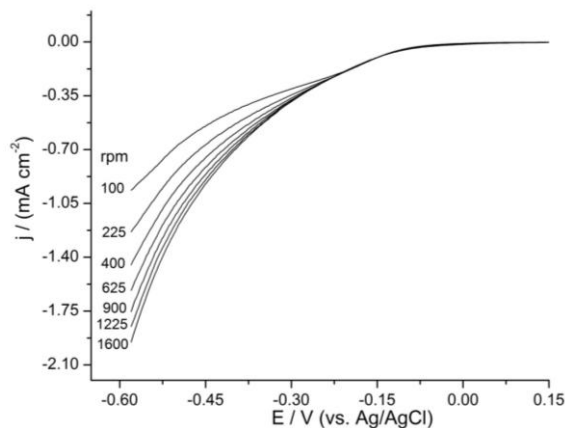
Figure 6b. Disk currents density (based on the geometric area of the glassy carbon electrode) at different rotation rates during the ORR in 0.1M TFMSA + 0.8 mM Mn(III)TMPyP. Scan rate: 20mV s^{-1}
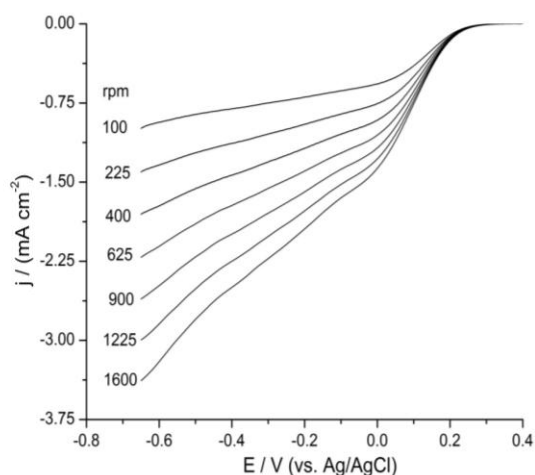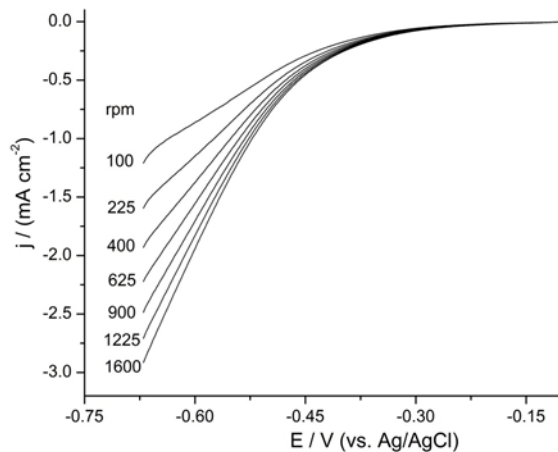

Figure 6c. Disk currents density (based on the geometric area of the glassy carbon electrode) at different rotation rates during the ORR in 0.1M TFMSA + 0.8 mM Co(III)TMPyP. Scan rate: 20mV s^{-1}

Figure 6d. Disk currents density (based on the geometric area of the glassy carbon electrode) at different rotation rates during the ORR in 0.1M TFMSA + 0.6 mM Cu(II)TMPyP. Scan rate: 20mV s^{-1}

With the above information, the standard rate constant (k_I) for ORR by Fe(III)/Fe(II)TMPyP was determined, and so did for the other M^*/M'TMPyP (M^*/M' = Co(III)/Co(II), Mn(III)/Mn(II) and Cu(II)/Cu(I))as listed in Table 1. Fig. 8 shows variations of log k_I *vs*. E^0 for the catalyst complexes. The slope of -1/125 mV reflects the intrinsic kinetics of the reaction with O_2 as it varies with potential [33]. Based on Marcus theory [33, 44], the theoretical variation of k_I with E^0 has a linear relationship with a slope of -1/60 mV in the diffusion-control region and a slope of -1/120 mV in the activation-control region.
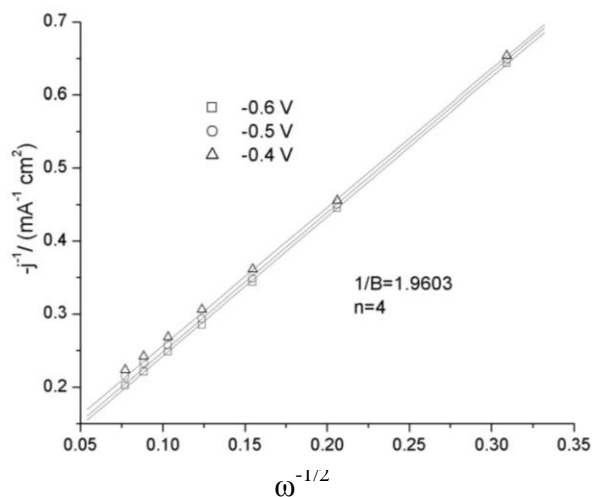

Figure 7a. Koutechy-Levich plots for oxygen reduction at different potentials in O_2 saturated 0.1M TFMSA + 0.8 mM Fe(III)TMPyP
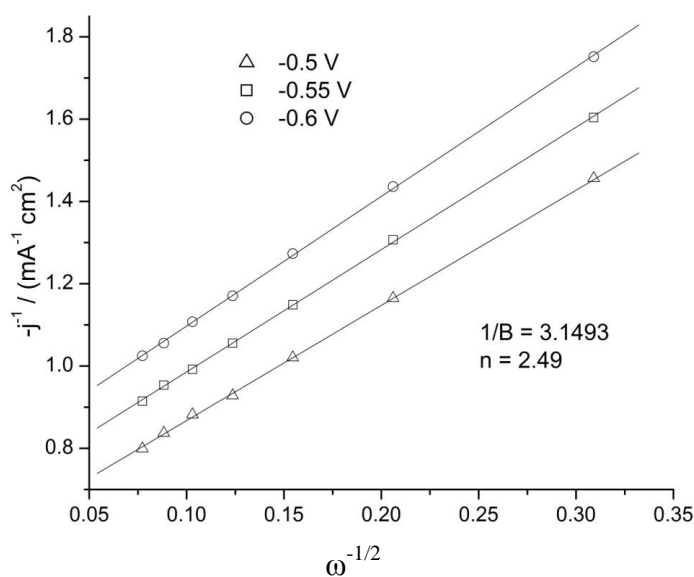

Figure 7b. Koutechy-Levich plots for oxygen reduction at different potentials in O_2 saturated 0.1M TFMSA + 0.8 mM Mn(III) complex
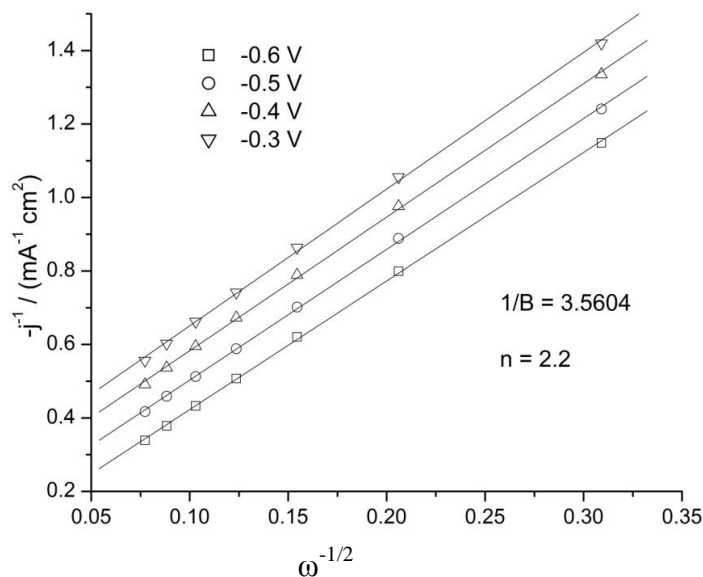
Figure 7c. Koutechy-Levich plots for oxygen reduction at different potentials in O_2 saturated 0.1M TFMSA + 0.8 mM Co(III) complex
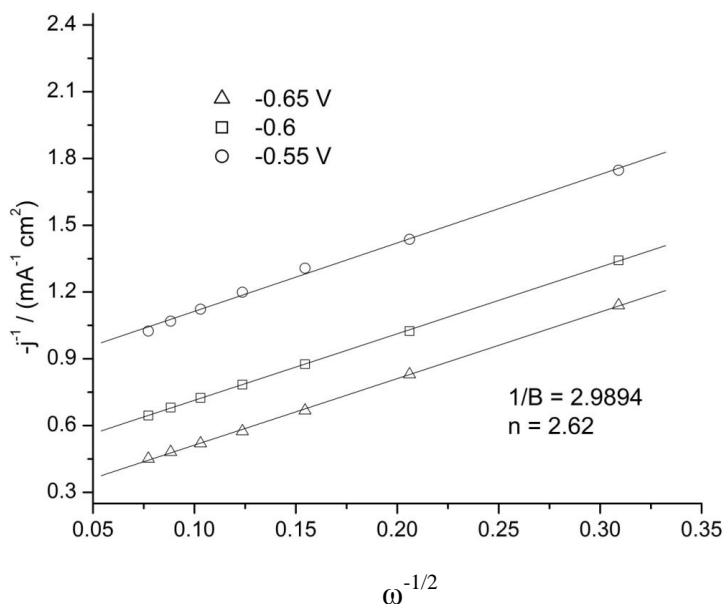

Figure 7d. Koutechy-Levich plots for oxygen reduction at different potentials in O_2 saturated 0.1M TFMSA + 0.6 mM Cu(II) complex

The observed experimental slope value of -1/125 mV indicates that outer-sphere electron transfer may occur in an intermediate zone of activation control. However, the potential differences among the catalysts (Fig. 8) and the standard potential for superoxide formation ($E^0(O_2/O_2^{\bullet-})$ = -0.36V vs. NHE) appear to be quite large [50, 51]. In addition, no experimental data are available in the diffusion region wherein one could make a linear extrapolation of the -1/60 mV line to achieve and evaluate the value of k_I for $\Delta G^0 = 0$ [52]. As a result, an inner-sphere mechanism is also proposed with

the postulation of formation of a bond between the reduced redox metal complex and O_2. The reaction sequence involving O_2 binding to a central metal ion with low valence followed by protonation and a second electron transfer is outlined in reactions (a') to (e'). For iron porphyrin, the produced H_2O_2 can be further reduced to water through reactions (f') to (j'), accompanied by the formation of a new porphyrin-oxygen intermediate complex [53, 54].
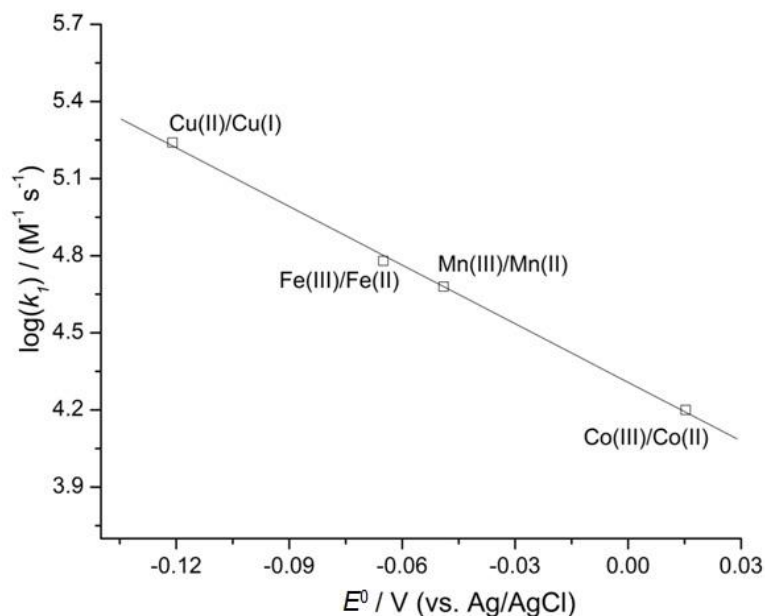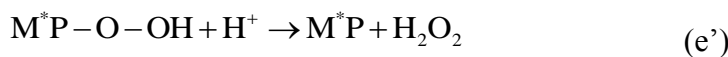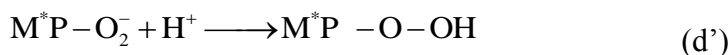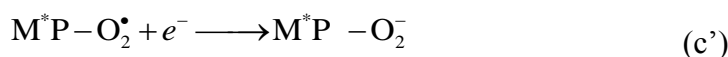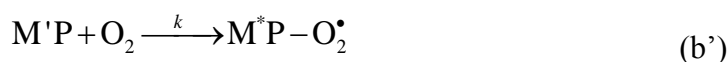

Figure 8. k_1 as a function of formal potential E^0 for the oxygen reduction reaction by metal porphyrins

In fact, the ORR benefits from the favorable inner-sphere pathway due to a lower reorganization barrier [49, 55-57].

$$M^*P + e^- \leftrightarrow M'P \tag{a'}$$

$$M'P + O_2 \xrightarrow{k} M^*P - O_2^\bullet \tag{b'}$$

$$M^*P - O_2^\bullet + e^- \longrightarrow M^*P - O_2^- \tag{c'}$$

$$M^*P - O_2^- + H^+ \longrightarrow M^*P - O - OH \tag{d'}$$

$$M^*P - O - OH + H^+ \rightarrow M^*P + H_2O_2 \tag{e'}$$

$$M^*P + e^- \leftrightarrow M'P \tag{f'}$$

$$M'P + H_2O_2 \rightarrow M^*P - O^\bullet + H_2O \tag{g'}$$

$$M^*P - O^\bullet + e^- \rightarrow M^*P - O^- \tag{h'}$$

$$M^*P - O^- + H^+ \longrightarrow M^*P - OH \tag{i'}$$

$$M^*P - OH + H^+ \rightarrow M^*P + H_2O \tag{j'}$$
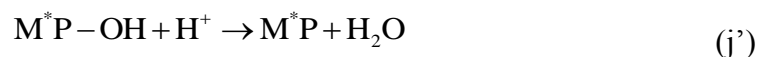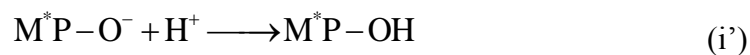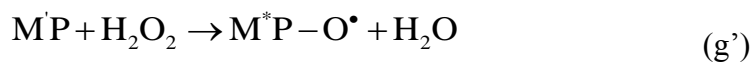
In the equations above, M^*P and $M'P$ are general symbols for the metal porphyrins and reduced metal porphyrins, respectively.

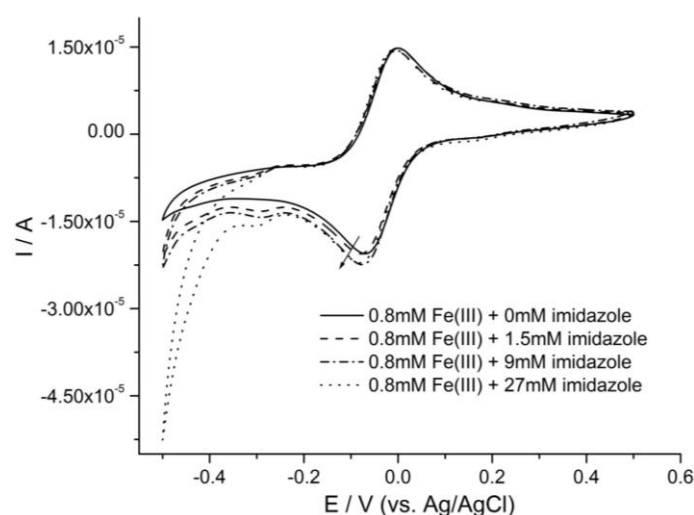**Figure 9.** Cyclic voltammograms on a glassy carbon in Ar-purged 0.1M TFMSA containing 0.8mM Fe(III)TMPyP with different concentrations of imidazole, scan rate = 50mV s^{-1}
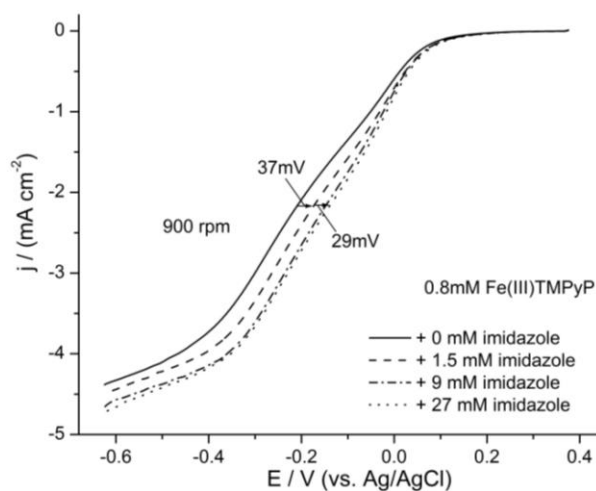

Figure 10. Disk current density at 900 rpm during ORR in 0.1M TFMSA containing 0.8mM Fe(III)TMPyP with different concentrations of imidazole, scan rate = 20mV s^{-1}

From both the outer-sphere (c1-c6) and inner-sphere (a'- e') mechanisms, the protonation reactions are critical steps successive to the formation of $O_2^{\bullet-}$ radicals or bond formation between reduced transition metals and O_2. Consequently, it is of great interest to examine the effect of proton activity on the performance of the above redox catalysts for ORR. In this study, imidazole was chosen as the additive in the TFMSA + metal complexes system due to its capability for proton activation and conduction [58]. Fig. 9 shows the cyclic voltammograms of a glassy carbon electrode in 0.1 M TFMSA + 0.8 mM Fe(III)TMPyP with different concentrations of imidazole (in Ar purged solutions). There is no significant change for the oxidation and reduction peaks associated with the Fe(III)/Fe(II) redox couple, because the imidazole is protonated under these conditions and does not bind to the complex. This result implies that the electronic density on the transition metals does not change, given the evidence that the pH of the solution remained constant after addition of imidazole (up to 27 mM). In contrast, an appreciable difference was observed on the ORR polarization curves in oxygen-saturated 0.1 M TFMSA with the addition of various amounts of imidazole as shown in Fig. 10. The half-wave potentials ($E_{1/2}$) exhibited an apparent anodic shift with increasing concentration of imidazole without the onset potential change. This behavior clearly indicates that imidazole promotes faster turnover frequencies of the ORR, presumably by activating protons during the homogeneous catalysis process with transition metal redox catalysts. The detailed study of the proton-activation effect on homogeneously catalyzed ORR by varying the pH and adding different amounts of proton-solvating compounds (*e.g.* imidazole, bispyridine, *etc*) will be the subject of forthcoming publications.

The reactivity of the metal complexes in MEAs of the PEMFCs is predicted by calculating the average turnover frequency (TOF). It is considered that the thin redox polymer is deposited on the spherical carbon catalyst support (the radius, r_{cs} of 50 nm), and these are tightly packed in the 10 μm thick catalyst layer, L_{CL}, as shown in Fig. 1. The reaction occurs only at the redox polymer, and its current density, i_{CAT}, is predicted using the available model to represent reactions (a) to (c) above[59]. The diffusivities of electron and oxygen used are $D_e = 1 \times 10^{-9}$ cm^2 s^{-1} [60] and $D_{O_2} = 0.6 \times 10^{-6}$ cm^2 s^{-1} [61], and the concentration of catalyst sites is $c_p = 1.328$ mol cm^{-3}. The oxygen is provided through the thin liquid-water layer from the pores in the catalyst layer. The oxygen concentration of 1.6×10^{-6} mol cm^{-3} was determined at the boundary, including Knudsen diffusion [60]. The volumetric current source, $\nabla \cdot i$, is predicted by the specific surface area of the spherical particles (varying with the film thickness, L_δ) and the current density from the polymer i_{CAT} given as

$$\nabla \cdot i = (A/V) i_{CAT} \qquad (3)$$

The average turnover frequency is predicted by the average volumetric current source and the catalytic site density (varying with the film thickness, L_δ).

Fig. 11 shows the variations of the average TOF with respect to the catalyst-layer thickness at $E°$ (Fig. 8). The film thickness determines the balance between kinetic and electron/oxygen diffusion limitations. The thin film kinetically limits current density due to the limited reaction sites, whereas the thick film hinders electron/oxygen diffusion. The maximum TOF (reactivity) are 14.2 and 1.8 s^{-1} with the optimal film thickness at 60 and 150 nm for Cu(II)/Cu(I) and Co(III)/Co(II), respectively. The

optimal thickness increases as the reaction-rate decreases since it requires an increased number of the reaction sites.
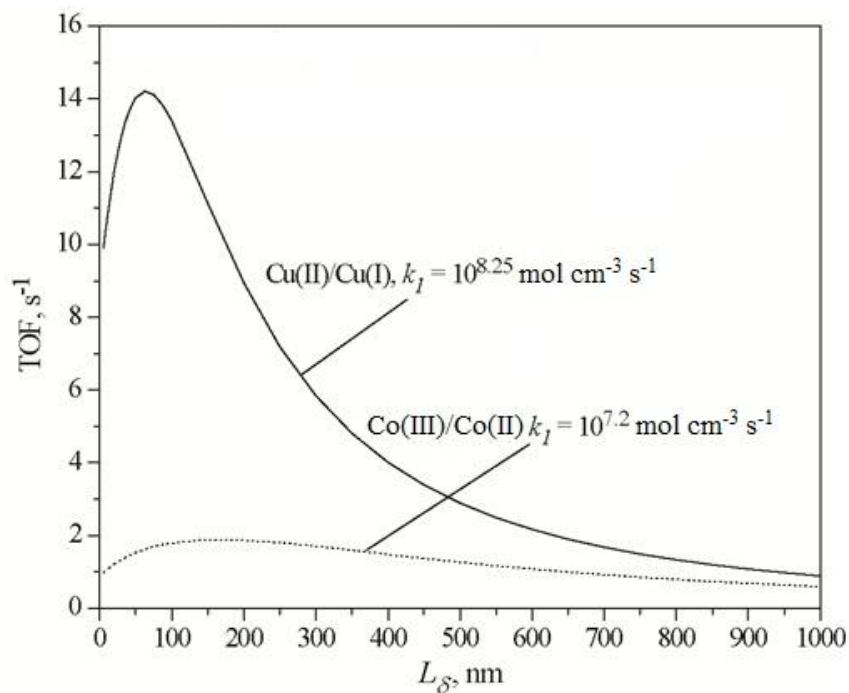

Figure 11. Variations of the average TOF of the polymer catalysts, Cu(II)/Cu(I) and Co(III)/Co(II) at E° (Figure 8) as a function of the film thickness, L_δ.

4. CONCLUSIONS

The oxygen-reduction-reaction (ORR) kinetics and catalytic activity of the water-soluble metal-porphyrin complexes M*TMPyP (M* = Fe(III), Co(III), Mn(III) and Cu(II)), in 0.1 M TFMSA were examined. Except for Cu(II)TMPyP, no evidence of irreversible adsorption of metal complexes was found on the glassy carbon electrode. For the ORR, the onset potential is closely related to the redox potential of M*TMPyP, exhibiting an "ECE" working mechanism. A model for outer-sphere catalysis involving superoxide ions ($O_2^{\bullet-}$) as the initial species of the ORR followed by protonation reactions appears likely by inspecting the linearity and slopes of a variation of the rate constant k_1 with the formal potential E^0 of the redox couples. However, an inner-sphere electron transfer mechanism cannot be ruled out at this stage. The proposed model for the formation of a complex between M'TMPyP (M' = Fe(II), Co(II), Mn(II) and Cu(I)) with O_2 shows that for both outer-/inner-sphere mechanisms the protonation reactions may result in high turnover frequencies. In support of this point is the observation that the catalytic activity of the Fe(III)TMPyP redox catalyst was markedly enhanced by the addition of imidazole with the capability for proton activation. Detailed studies of similar effects may yield further insight into the nature of the ORR catalyzed by homogeneous redox catalysts. In the catalyst layer, a macroscopic model shows that the electrochemical reaction is maximized at the film thickness of 60 and 150 nm for Cu(II)/Cu(I) and Co(III)/Co(II), and the optimal

thickness increases as the reaction-rate decreases. Using the macroscopic model, the results suggest that the 3-D redox polymer catalyst with an optimal geometry is a good candidate to replace the noble metal catalysts used in the practical electrochemical cells.

References

1. B.C.H. Steele and A. Heinzel, *Nature*, 414 (2001) 345.
2. J. Xie, D.L. Wood, III, K.L. More, P. Atanassov and R.L. Borup, *J. Electrochem. Soc.*, 152 (2005) A1011.
3. V.S. Murthi, R.C. Urian and S. Mukerjee, *J. Phys. Chem*. B, 108 (2004) 11011.
4. G. Brumfiel, *Nature*, 422 (2003) 104.
5. D.J. Berger, *Science*, 286 (1999) 49.
6. Q. He, X. Yang, X. Ren, B.E. Koel, N. Ramaswamy, S. Mukerjee and R. Kostecki, *Journal of Power Sources*, 196 (2011) 7404.
7. Z.P. Li and B.H. Liu, *Journal of Applied Electrochemistry*, 40 (2010) 475.
8. S. Pylypenko, S. Mukherjee, T.S. Olson and P. Atanassov, *Electrochim. Acta*, 53 (2008) 7875.
9. Q. He, X. Yang, R. He, A. Bueno-Lopez, H. Miller, X. Ren, W. Yang and B.E. Koel, *Journal of Power Sources*, 213 (2012) 169.
10. D. Susac, A. Sode, L. Zhu, P.C. Wong, M. Teo, D. Bizzotto, K.A.R. Mitchell, R.R. Parsons and S.A. Campbell, *J. Phys. Chem*. B, 110 (2006) 10762.
11. L. Zhu, D. Susac, A. Lam, M. Teo, P.C. Wong, D. Bizzotto, S.A. Campbell, R.R. Parsons and K.A.R. Mitchell, *J. Solid State Chem*., 179 (2006) 3942.
12. R.A. Sidik and A.B. Anderson, *J. Phys. Chem*. B, 110 (2006) 936.
13. E. Vayner, R.A. Sidik, A.B. Anderson and B.N. Popov, *J. Phys. Chem*. C, 111 (2007) 10508.
14. Y. Feng, T. He and N. Alonso-Vante, *Chem. Mater*., 20 (2008) 26.
15. R. Bashyam and P. Zelenay, *Nature* , 443 (2006) 63.
16. V.G. Khomenko, V.Z. Barsukov and A.S. Katashinskii, *Electrochim. Acta*, 50 (2005) 1675.
17. M. Yuasa, H. Murata, K. Ikkanda, K. Tanaka, T. Imai and K. Oyaizu, *Mater. Technol*., 25 (2007) 313.
18. Y. Ji, Z. Li, S. Wang, G. Xu and X. Yu, *Int. J. Hydrogen Energy*, 35 (2010) 8117.
19. J.A.R. Van Veen and H.A. Colijn, Ber. Bunsenges. *Phys. Chem*., 85 (1981) 700.
20. J.A.R. Van Veen, J.F. Van Baar, C.J. Kroese, J.G.F. Coolegem, N. De Wit and H.A. Colijn, Ber. Bunsenges. *Phys. Chem*., 85 (1981) 693.
21. [H.A. Gasteiger, S.S. Kocha, B. Sompalli and F.T. Wagner, *Appl. Catal*., B, 56 (2005) 9.
22. J.P. Collman, N.K. Devaraj, R.A. Decreau, Y. Yang, Y.-L. Yan, W. Ebina, T.A. Eberspacher and C.E.D. Chidsey, *Science*, 315 (2007) 1565.
23. C.J. Chang, L.L. Chng and D.G. Nocera, *J. Am. Chem. Soc*., 125 (2003) 1866.
24. C.J. Chang, Z.-H. Loh, C. Shi, F.C. Anson and D.G. Nocera, *J. Am. Chem. Soc*., 126 (2004) 10013.
25. C.J. Chang, Y. Deng, D.G. Nocera, C. Shi, F.C. Anson and C.K. Chang, *Chem. Commun*., (2000) 1355.
26. J.A. Cracknell, K.A. Vincent and F.A. Armstrong, *Chem. Rev*., 108 (2008) 2439.
27. E. Vayner, H. Schweiger and A.B. Anderson, *J. Electroanal. Chem*., 607 (2007) 90.
28. H. Schweiger, E. Vayner and A.B. Anderson, *Electrochem. Solid-State Lett*., 8 (2005) A585.

29. J.-M. Saveant, *Chem. Rev.*, 108 (2008) 2111.
30. J.B. Kerr, L.L. Miller and M.R. Van de Mark, *J. Am. Chem. Soc*., 102 (1980) 3383.
31. J.B. Kerr and L.L. Miller, *J. Electroanal. Chem. Interfacial Electrochem*., 101 (1979) 263.
32. F.C. Anson, C.L. Ni and J.M. Saveant, *J. Am. Chem. Soc*., 107 (1985) 3442.
33. C.P. Andrieux, C. Blocman, J.M. Dumas-Bouchiat and J.M. Saveant, *J. Am. Chem. Soc*., 101 (1979) 3431.
34. C.P. Andrieux, O. Haas and J.M. Saveant, *J. Am. Chem. Soc.,* 108 (1986) 8175.
35. Q. He, T. Mugadza, X. Kang, X. Zhu, S. Chen, J. Kerr and T. Nyokong, *Journal of Power Sources,* 216 (2012) 67.
36. P.A. Forshey and T. Kuwana, *Inorg. Chem*., 20 (1981) 693.
37. T. Kuwana, M. Fujihira, K. Sunakawa and T. Osa, *J. Electroanal. Chem. Interfacial Electrochem.*, 88 (1978) 299.
38. C.-H. Yu and Y.O. Su, *J. Electroanal. Chem*., 368 (1994) 323.
39. H.L. Smith, R.L. Usala, E.W. McQueen and J.I. Goldsmith, *Langmuir,* 26 (2010) 3342.
40. L. Ruhlmann, J. Zimmermann, W. Fudickar, U. Siggel and J.H. Fuhrhop, *J. Electroanal. Chem.*, 503 (2001) 1.
41. M.-h. Liu and Y.O. Su, *J. Electroanal. Chem*., 426 (1997) 197.
42. C.P. Andrieux, J.M. Dumas-Bouchiat and J.M. Saveant, *J. Electroanal. Chem. Interfacial Electrochem*., 87 (1978) 39.
43. C.P. Andrieux, J.M. Dumas-Bouchiat and J.M. Saveant, *J. Electroanal. Chem. Interfacial Electrochem.*, 88 (1978) 43.
44. C.P. Andrieux, J.M. Dumas-Bouchiat and J.M. Saveant, *J. Electroanal. Chem. Interfacial Electrochem.,* 87 (1978) 55.
45. A. Bettelheim and T. Kuwana, *Anal. Chem*., 51 (1979) 2257.
46. C.P. Andrieux, C. Blocman, J.M. Dumas-Bouchiat, F. M'Halla and J.M. Saveant, *J. Electroanal. Chem. Interfacial Electrochem*., 113 (1980) 19.
47. C.P. Andrieux, J.M. Dumas-Bouchiat and J.M. Saveant, *J. Electroanal. Chem. Interfacial Electrochem.*, 113 (1980) 1.
48. P.N. Ross and P.C. Andricacos, *J. Electroanal. Chem. Interfacial Electrochem*., 154 (1983) 205.
49. R.J.H. Chan, Y.O. Su and T. Kuwana, *Inorg. Chem.*, 24 (1985) 3777.
50. I. Afanas′ev, Superoxide ion: chemistry and biological implications, Boca Raton : CRC Press, 1989.
51. J.H. Baxendale, M.D. Ward and P. Wardman, *Trans. Faraday Soc*., 67 (1971) 2532.
52. A. Gennaro, A.A. Isse, J.-M. Saveant, M.-G. Severin and E. Vianello, *J. Am. Chem. Soc*., 118 (1996) 7190.
53. P.A. Forshey and T. Kuwana, *Inorg. Chem*., 22 (1983) 699.
54. C.F. Kolpin and H.S. Swofford, Jr., *Anal. Chem*., 50 (1978) 920.
55. K. Kumar, F.P. Rotzinger and J.F. Endicott, *J. Am. Chem. Soc.,* 105 (1983) 7064.
56. B. Durham, J.F. Endicott, C.-L. Wong and D.P. Rillema, *J. Am. Chem. Soc*., 101 (1979) 847.
57. F.P. Rotzinger, K. Kumar and J.F. Endicott, *Inorg. Chem*., 21 (1982) 4111.
58. X.-G. Sun, J.B. Kerr, G. Liu and C.L. Reeder, *Prepr. Symp. - Am. Chem. Soc., Div. Fuel Chem.*, 49 (2004) 596.
59. C.P. Andrieux, J.M. Dumas-Bouchiat and J.M. Saveant, *J. Electroanal. Chem. Interfacial Electrochem.*, 114 (1980) 159.
60. B.A. White and R.W. Murray, *J. Am. Chem. Soc.,* 109 (1987) 2576.
61. A.T. Haug and R.E. White, *J. Electrochem. Soc.*, 147 (2000) 980